Visualizing the Frontier Orbitals of a Conformationally Adapted Metalloporphyrin

ARTICLE *in* CHEMPHYSCHEM · JANUARY 2008

Impact Factor: 3.42 · DOI: 10.1002/cphc.200700600 · Source: PubMed

DOI: 10.1002/cphc.200700600

Visualizing the Frontier Orbitals of a Conformationally Adapted Metalloporphyrin

Alexander Weber-Bargioni,*[a] Willi Auwärter,[c] Florian Klappenberger,[c] Joachim Reichert,[a] Simon Lefrançois,[a] Thomas Strunskus,[b] Christof Wöll,[b] Agustin Schiffrin,[a] Yan Pennec,[a] and Johannes V. Barth*[a, c]

We present a molecular-level study of the geometric and electronic properties of Co^{II} tetraphenylporphyrin molecules adsorbed on the Cu(111) surface. A combination of low-temperature scanning tunneling microscopy and near-edge X-ray absorption fine structure observations reveals how the metal substrate induces a conformational adaptation into a distorted saddle-shaped geometry. By scanning tunneling spectroscopy we identified the discrete energy levels of the molecule and mapped their spatial electron-density distributions. These results, along with a simple theoretical description, provide a direct correlation between the shape of frontier molecular orbitals and intramolecular structural features.

Introduction

The conformation of functional molecules frequently determines their physicochemical properties and their interaction with the local environment. Notably, metal-containing species in biological systems show a high degree of flexibility, whereby shape and functionality are intimately related.[1] A prominent class a prominent class of such molecules is the metalloporphyrins, which play a central role in life processes such as transport of respiratory gases, photosynthesis, and catalytic functions.[2,3] Distortions of the porphyrin macrocycle from planarity are the key to rationalizing their photophysical, chemical, and magnetic properties,[4] and they can be exploited for conformational design and development of novel biomimetic systems.[5] For the nanoscale control of such properties an understanding of the interplay between electronic properties and molecular conformation must be developed at the single-molecule level. Herein we present a study on the geometric and electronic properties of Co^{II} tetraphenylporphyrin (Co-TPP) molecules adsorbed on a well-defined Cu(111) surface. Combined low-temperature scanning tunneling microscopy and near-edge X-ray-absorption fine structure observations reveal how the metal substrate induces a conformational adaptation into a distorted saddle-shaped geometry. Using scanning tunneling spectroscopy we assessed the internal electronic structure of the molecule, identified its discrete energy levels, and mapped the corresponding spatial electron-density distributions. These results, along with a simple theoretical description, provide a direct correlation between the shape of frontier molecular orbitals and intramolecular structural features.

The charge densities from frontier molecular orbitals (MOs) of adsorbed molecules with π-conjugated electron systems can be related to their topographic appearance in scanning tunneling microscopy (STM) images.[6–9] Moreover, the spectral density of complex adsorbed species such as C_{60} was investigated by scanning tunneling spectroscopy (STS) studies with energy-selective mapping of individual MOs.[10,11] The rigid carbon backbone of C_{60} remains essentially preserved on adsorption.[12,13] By contrast, STM topographic features of adsorbed porphyrins indicate intramolecular distortions of varying extent on metal substrates,[14–17] and STM manipulation experiments provided indirect evidence for switching between different conformers.[18,19] Thus, there is a need to quantify the conformations of adsorbed flexible species and correlate them with their electronic structure. Firstly, this is decisive for a comprehensive understanding of adsorption phenomena and conformational adaptation at the single-molecule level. Secondly, such knowledge is a mandatory prerequisite to advance the engineering of molecular nanoarchitectures,[20] and to develop a rationale for conformational control of flexible species and supramolecular assemblies thereof.[21–23]

While metalloporphyrins on surfaces have been the subject of intensive research,[14,17,19,24–26] details of their electronic structure and the spatial characteristics of their individual MOs have hitherto remained elusive to experimental studies. Our high-resolution STM images reveal bias-dependent intramolecular features. With the help of near-edge X-ray absorption fine structure (NEXAFS) experiments the observed twofold symmetry was related to a molecular adsorption geometry with a saddle-shaped macrocycle. Using STS we distinguish the

[a] *A. Weber-Bargioni, Dr. J. Reichert, S. Lefrançois, A. Schiffrin, Dr. Y. Pennec, Prof. J. V. Barth*
Departments of Chemistry and Physics & Astronomy
The University of British Columbia, Vancouver BC V6T 1Z4 (Canada)
Fax: (+1) 60-4822 4750
E-mail: aweber@phas.ubc.ca

[b] *Dr. T. Strunskus, Prof. C. Wöll*
Lehrstuhl für Physikalische Chemie
Ruhr-Universität Bochum, Bochum (Germany)

[c] *Dr. W. Auwärter, Dr. F. Klappenberger, Prof. J. V. Barth*
Physik Department E20, TU München (Germany)
Fax: (+49) 89-289 12338
E-mail: jvb@ph.tum.de

energy levels of individual molecular orbitals and selectively map the shape of the pertinent electron-density distributions. Simulations based on semi-empirical extended Hückel theory (EHT) calculations confirm the link between the measured MO appearance and the molecular conformation.

Results and Discussion

Bonding and Ordering of Co-TPP on Cu(111)

A structural model of Co-TPP (Figure 1 a) shows the central porphyrin macrocycle with a fourfold-coordinated Co^{II} center. The phenyl moieties are free to rotate about the σ-bond axis

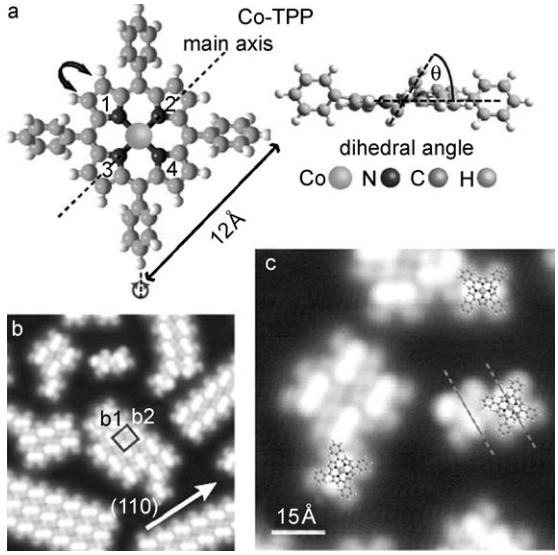

Figure 1. a) Model of an isolated Co-TPP molecule with definition of the main axis and the dihedral angle θ. A saddle-shaped distortion bends pyrrole rings 1 and 3 (2 and 4) down (up). b) Co-TPP islands on Cu(111) display a nearly square unit cell ($b_1 = 14.1$, $b_2 = 14.2$ Å). c) High-resolution image with intramolecular features revealing twofold symmetry ($V_t = -2.1$ V, $I = 0.1$ nA).

connecting them to the pyrrole units and can therefore adapt to the local environment. For free or weakly adsorbed molecules, the corresponding dihedral angles θ exceed 60°.[4,16] However, steric constraints interfere for dihedral angles below 60°, whereby the repulsive interactions between hydrogen atoms at phenyl *ortho* positions and adjacent pyrrole moieties induce marked distortions of the macrocycle.[4,5]

On depositing small amounts of Co-TPP on Cu(111), regular islands form with a nearly square unit cell, the extension of which reflects the size of the molecules ($b_1 = 14.1$, $b_2 = 14.2$ Å; see Figure 1 b). This packing scheme was similarly identified in metal-TPP assemblies on close-packed noble metal surfaces.[17,25] The high-resolution STM image depicted in Figure 1 c, obtained under conditions where a wide spectrum of occupied sample states contributes to the tunneling current, reveals distinct intramolecular features. We use the cigar-shaped protrusion over the macrocycle to define the main axis and associate the four smaller lateral protrusions with the *meso* groups.[16,17] The twofold symmetric appearance indicates that following adsorption the conformation of the molecules differs from that of the free species (in which the macrocycle has fourfold symmetry), that is, deformation of the macrocycle from planarity has occurred.

Adsorption-Induced Saddle-Shaped Molecular Conformation

In order to clarify the connection between STM topographic appearance and molecular conformation, NEXAFS experiments were carried out. With this technique the orientation of functional moieties with respect to the substrate plane can be assessed.[27] The spectra of the C 1s edge (Figure 2 a) consist of

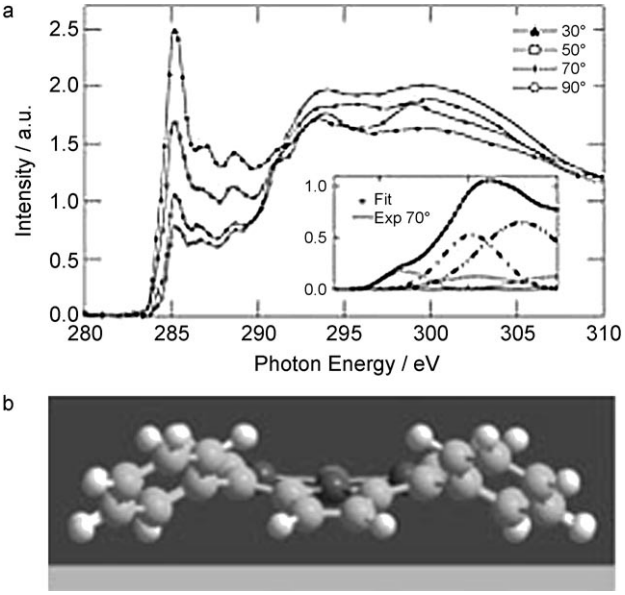

Figure 2. Saddle-shape conformational adaptation of Co-TPP. a) NEXAFS spectra of the C 1s edge of a Co-TPP monolayer on Cu(111) for different incidence angles ($\phi = 30$–$90°$) between the *E* vector of the synchrotron beam and the surface normal. Symbols do not represent data points but serve to differentiate angles. Inset: Exemplary zoom of the leading edge of the 70° spectra with fit components. Symbols represent data points, and the solid line indicates the fit. Resonances associated with the macrocycle (phenyl groups) are shown with dotted (dash-dotted) lines. b) Structural model for the conformational adaptation of Co-TPP on Cu(111) with a saddle-shaped distortion of the macrocycle and a dihedral angle of 35°.

three peaks (285, 286.5, 288 eV) in the π* region and two peaks (293, 300 eV) in the σ* region. We concentrated our analysis on the leading edge around 285 eV, for which a deconvolution is straightforward. Following the argumentation in references [28,29], where closely related systems were studied, we decomposed the spectra into two parts, one originating from the macrocycle and one from the phenyl rings. For fitting we used three Gaussian peaks (dotted lines, inset of Figure 2 a) with fixed intensity ratios and widths to approximate the macrocycle part.[28,29] In the same way two Gaussians served for the phenyl-related part (dash-dotted lines). Thus, for the fitting

procedure only two free parameters were used, that is, the intensities of the molecular subunits. The analysis of the angular dependence yielded values of about 35° (phenyl) and about 20° (macrocycle) for the angle between the corresponding π* dipole moment and the surface normal.

The nonzero macrocycle angle indicates distortion of the molecular backbone and is consistent with previously conjectured prominent saddle-shaped deformations for metal-TPPs on surfaces. This porphyrin conformation implies that one pair of opposite pyrrole rings tilts upwards, while the other pair bends down (see Figure 1 a).[4,5] Interpreting the NEXAFS data in terms of the saddle-shaped model, we find for Co-TPP a dihedral angle θ of approximately 35° and estimate the bending of the pyrrole rings to be ±20°. The resulting twofold macrocycle symmetry is consistent with both the STM observations and the geometry derived from basic semi-empirical calculations, as shown in Figure 2 b (the saddle-shaped deformation was obtained by optimizing the geometry of the macrocycle with the semi-empirical PM3 method complying with the constraints given by the phenyl orientation).

Electronic Structure and Charge Density Distribution of Frontier Orbitals

A comparison of the STM topographs reproduced in Figures 3 a,d and 1 reveals strongly bias dependent appearance of intramolecular features. Marked differences exist between images reflecting occupied and unoccupied electronic states obtained at negative and positive bias voltages, respectively. For instance, the dominant cigar-shaped protrusion resolved at $V_t = -2.1$ V (Figure 1 c) transforms into an oval bright core at $V_t = -400$ mV (Figure 3 d). On tunneling into the unoccupied states ($V_t = 800$ mV, see Figure 3 a), we resolve bright lobes localized over the four *meso* bridge carbon atoms and a local central depression. This changing appearance indicates contributions of different electronic channels to the tunneling current arising from the local density of states (LDOS) associated with MOs.[16,25,30] We thus explored the pertinent electronic properties by STS. Spectra averaging over several molecules are shown in Figure 3 b. The orange curve represents the raw d*I*/d*V* data, whereas the green curve was obtained by normalization, that is, dividing by *I*/*V*. The latter reveals more detailed features (i.e., local maxima) that do not exist for the pristine copper surface. Based on their appearance in spatially resolved electron-density maps, as described below, we assign the adsorbed Co-TPP HOMO to the peak at −350 mV (blue dashed line) and the LUMO to the peak at 420 mV [red dashed line; referenced to the Fermi level ($V_t = 0$)]. Thus, we define the first state at positive (negative) bias voltages in the tunneling spectrum as LUMO (HOMO), the second as LUMO−1 (HOMO+1), and so on, which notation does not discriminate between molecular orbitals solely related to the organic moieties and states with strong metal-center d character and thus deviates from alternative definitions. This indicates a marked reduction of the HOMO–LUMO gap to 770 mV, significantly smaller than the gap of 1.4 eV for planar conformers suggested from optical absorption spectra[31] (for comparison, DFT calculations indicated 2.5 eV[32]). Similar reductions were reported for simpler systems[9] and can be ascribed to surface polarization effects.[33,34] The interaction with the surface also accounts for the broaden-

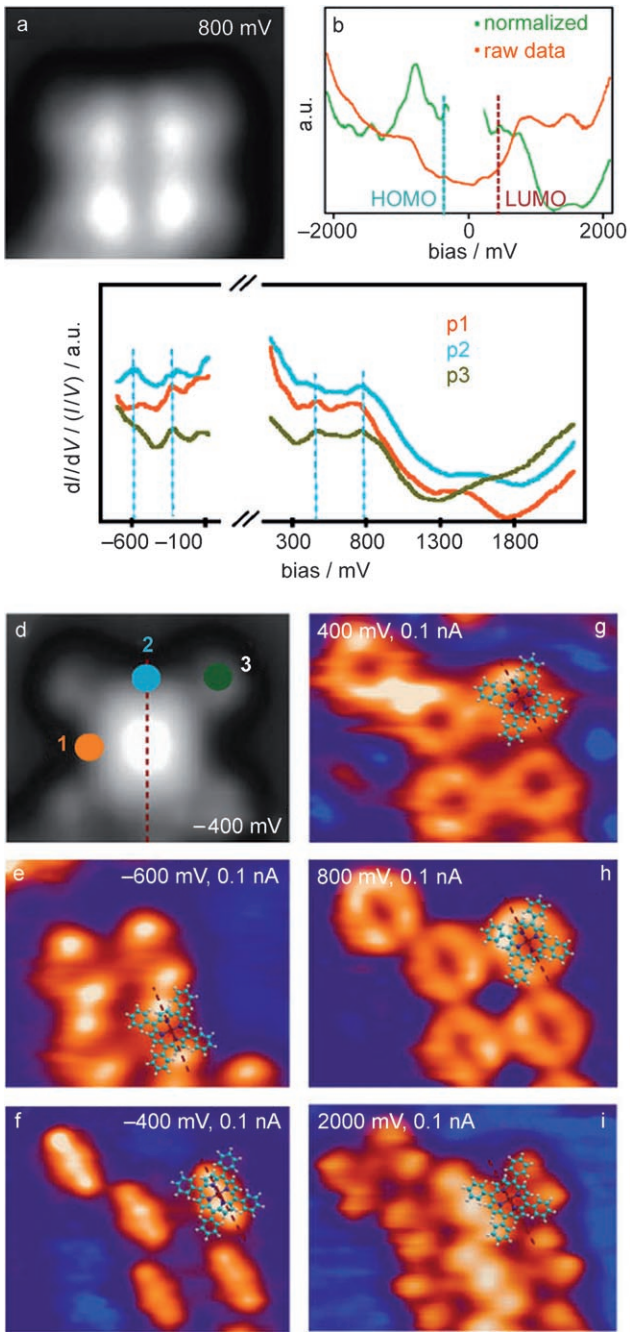

Figure 3. Inhomogeneous electronic structure and identification of frontier orbitals. a, d) Contrast change in STM topographs for tunneling into occupied and unoccupied states, respectively (both $I = 0.25$ nA). b) Tunneling spectrum averaged over several molecules, whereby the orange curve represents raw data and the green curve is normalized (d*I*/d*V* divided by *I*/*V*); initial conditions: $V_t = -2.1$ V, $I = 0.2$ nA. c) Normalized spectra at the three positions over the molecule indicated in d), whereby 1 and 2 are different locations at the macrocycle, and 3 is right at the phenyl group. Frontier MO energy levels are marked by dashed lines. e–i) Visualization of the spectral density of molecular orbitals by d*I*/d*V* mapping. The maps confirm the laterally varying signature of the line spectra.

ing of the discrete levels of the isolated molecules into the observed resonances displaying energy widths of 100–400 mV. Interestingly, for the related tetrapyridylporphyrin species adsorbed on the same substrate, for which even stronger intramolecular distortions occur, the molecular resonances could not be identified in STS, although the molecular appearance in STM clearly indicated tunneling mediated by molecular orbitals.[35]

To identify the frontier orbitals of Co-TPP and discriminate the position dependence of tunneling current contributions from different conduction channels, we recorded tunneling spectra at selected sites over the molecule (Figure 3c). They show a sequence of local maxima reflecting the LDOS at the molecule. There are occupied states close to the Fermi level, at energies of -350 and -600 meV, and unoccupied states at $+420$ and $+800$ meV. Furthermore, the STS measurements reflect marked intramolecular spatial variations: spectra p1 and p2 taken on dissimilar pyrrole groups (marked in Figure 3c) do not match and are very different from spectrum p3 taken on a phenyl end group (cf. Figure 3d). The data also reveal that the occupied states at negative bias appear with different weight. This explains the electronic asymmetry of the macrocycle reflected in the twofold-symmetric topography and substantiates the NEXAFS interpretation of a conformational adaptation.

The spatial characteristics of the frontier MOs were probed by d*I*/d*V* mapping. The data reproduced in Figure 3e–i were recorded at bias voltages for which STS identified discrete energy levels (dashed lines in Figure 3c; because we achieved the clearest contrast for the first molecular level below the Fermi energy at -400 mV, we use this d*I*/d*V* map as representation of the HOMO. Note that the intrinsic energy spread and applied bias modulation account for frontier MO maps of similar shape over an energy width of typically about 100 mV. We also took reference maps to probe the possible interference of the Cu(111) surface-state 2D electron gas, which due to the associated characteristic standing wave patterns in the vicinity of the Co-TPP islands could be clearly differentiated from the MO contributions. The occupied HOMO-1 state at -600 mV features a protrusion at each pyrrole group on the main axis (see overlaid model in Figure 3e). The HOMO in Figure 3f similarly displays a distinct twofold symmetry, but now with an intensity maximum at the Co-TPP center. Hence the occupied states account for the cigar-shaped protrusion along the main axis resolved in topographic data (see Figures 1c and 3d). In Figure 3g–i maps of the unoccupied states are reproduced. A toroidal shape is dominant for both $+400$ and $+800$ mV, whereby the first d*I*/d*V* map represents the LDOS associated with the LUMO and the $+800$ mV LUMO$+1$ resonance features a double-lip shape. This data sequence strongly suggests that the observed contours reflect the electron densities associated with individual frontier MOs. For higher unoccupied (and lower occupied) levels substantial peak broadening renders distinction of the respective MO contribution more difficult. However, with higher voltages ($V_t > 1$ V) a further clear change in symmetry and shape occurs, whereby the weight is shifted to the location of the phenyl substituents. An exemplary map is reproduced in Figure 3i.

Discussion of Tunneling Spectroscopy Maps

The spectroscopic signature and selective mapping of the Co-TPP frontier orbitals strongly suggest that the molecular electron system is largely decoupled from that of the metal substrate.[9,33,34] In agreement, a recent DFT investigation reported noncovalent bonding of transition metal porphines on Au(111).[26] However, the size of the present system prevents first-principles analysis.[36] For a first-order approximation we thus calculated MO maps for isolated Co-TPP in the framework of extended Hückel theory (EHT), which is known to reproduce the shape of molecular orbitals quite accurately, and electron density contours derived therefrom proved useful for the interpretation of STM topographic data of weakly bound complex adsorbates.[7,16,37,38] These simulations tacitly assume that the Cu(111) substrate mainly modifies the alignment of frontier orbital energies and broadens discrete molecular levels into resonances.[34] We considered distorted versus planar macrocycle conformers in order to assess their role in the observed dissymmetry. The saddle-shaped molecular structure was modeled by using the NEXAFS parameter set with the phenyl rings fixed at a dihedral angle of $\theta = 35^\circ$ and subsequent macrocycle relaxation yielding pyrrole-moiety tilts of $\pm 20^\circ$ (cf. Figure 2b).

The mimicked d*I*/d*V* maps reflect charge densities obtained by summing over nearly degenerate states. The comparison between the planar (Figure 4a–e) and saddle-shaped conformer (Figure 4f–j) reveals a similar MO sequence in both cases that reproduces the gross characteristics of the changing LDOS in the experimental findings (Figure 4k–o). However, the distinct symmetry break in the maps can be exclusively explained by the distorted molecular geometry. It is most pronounced for the electron-density distribution of the mapped occupied states (Figure 4i,n and j,o). Moreover, the differences in electron density at the Co^{II} center hint at a sequence reversal of the HOMO and HOMO-1 orbitals. On the one hand, this might be related to limitations of EHT in the description of metal–ligand interactions; DFT calculations on isolated Co-TPP indeed show that HOMO and HOMO-1 orbitals bear strong Co d-electron character.[32] On the other hand, the nature of d-like orbitals is affected by axial ligands,[32] and to some extent by the presence of a metal substrate.[25,26,39] These subtle effects are similarly understood as a possible reason for the present remarkable absence of an STS signature right at the Fermi level that could be associated with a Kondo resonance and thus a magnetic moment of the Co center, and that conversely was observed for a bromophenyl-substituted Co porphyrin on the same substrate.[24] Also the unoccupied MOs located at the phenyl substituents (Figure 4f,k) clearly reveal the symmetry break and reproduce the envelope of the corresponding STS map, although the experimentally observed electron density at the center of the adsorbed molecule does not exist for free Co-TPP.

Overall, the simple EHT description and STS mapping results can be reconciled and help to rationalize the observed spectral electron-density distributions with distinct symmetry. However, a more sophisticated theoretical analysis is clearly required for a comprehensive description of the system. Thereby it would

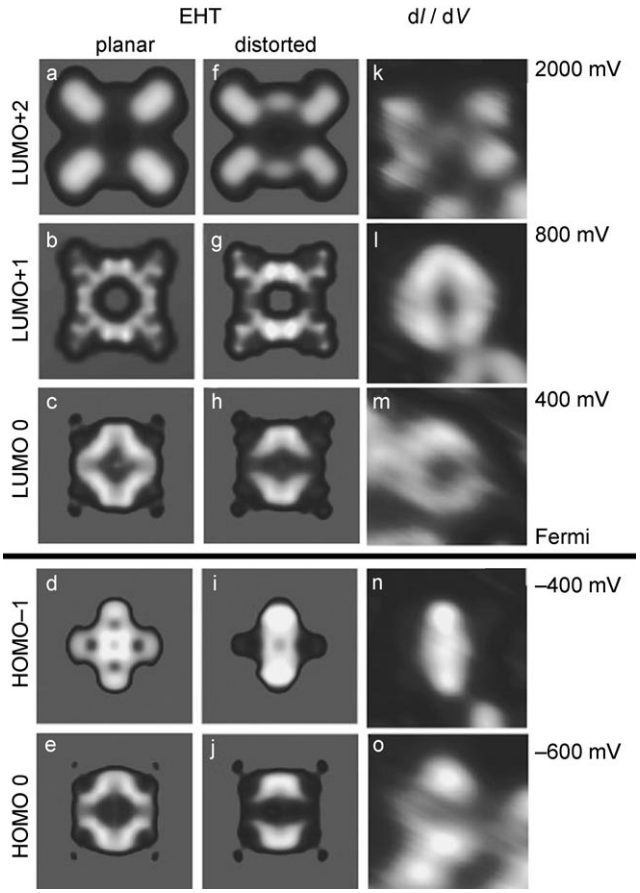

Figure 4. Calculated versus measured inhomogeneous electron density distributions of molecular orbitals. Comparison of EHT calculations of molecular orbitals for Co-TPP with planar macrocycle (a–e), the saddle-shaped conformer (f–j), and STS d*I*/d*V* maps (k–o). Shape and symmetry of experimental MOs are nicely reproduced by the calculations for the surface-adapted conformation, while the match with orbitals from undistorted molecules is less satisfactory

be desirable to address concurrently the electronic structure of the entire molecule–substrate complex and the interactions and energetics driving the conformational adaptation of Co-TPP, which implies orientation of the phenyl π-electron systems and lowering of the macrocycle plane towards the surface.

Conclusions

The interplay between molecular flexibility and electronic characteristics was investigated by STM and NEXAFS experiments in combination with extended Hückel theory calculations for Co-TPP molecules adsorbed on Cu(111). The visualization of frontier molecular orbitals with distinct symmetry by tunneling spectroscopy mapping reflects a saddle-shaped deformation, which is in agreement with the analysis of NEXAFS data. Our combination of techniques demonstrates the potential to provide deeper insight into conformational adaptation and its effect on electronic structure. This knowledge contributes to an improved understanding and control of flexible functional molecular species anchored on surfaces. It also opens up new vistas for tuning the functional properties of active metal centers in adaptive coordination units and for conformational design of molecular nanosystems and biomimetic materials.

Experimental Section

STM and STS experiments were performed with a custom-designed ultrahigh-vacuum apparatus ($p < 2\times10^{-10}$ mbar) comprising a commercial low-temperature scanning tunneling microscope (http://www.lt-stm.com/) typically operated at 10 K. The Cu(111) single crystal was prepared by repeated Ar^+ sputter–anneal cycles. Subsequently, Co-TPP was deposited from a Knudsen cell while the sample was held at 270 K. The indicated imaging bias voltages were applied to the sample. Differential conductance (d*I*/d*V*) data were obtained by lock-in amplifying technique with a modulation amplitude of 10 mV rms and a frequency of 1.3 kHz. The feedback loop was open for spectroscopy and closed for d*I*/d*V* mapping. The employed electrochemically etched W tip was shaped by controlled dipping into the substrate until intramolecular features were clearly resolved and reference spectra of the metal substrate yielded the Cu(111) electronic structure. The presented STS data could thus be obtained reproducibly. Varying the stabilizing tunneling current over two orders of magnitude probed the influence of the tip–sample distance on the d*I*/d*V* data, whereby no significant change could be observed. NEXAFS measurements were performed at the HE-SGM beamline at BESSY II using monolayer Co-TPP films deposited on Cu(111) after checking surface cleanliness by photoelectron spectroscopy. Data recording and processing followed procedures outlined elsewhere.[40] For the MO calculations with the semi-empirical extended Hückel method a commercial software package was employed (HYPERCHEM, Hypercube Inc., 1115 NW 4th street, Gainesville, Florida 32601). For the pertinent molecular relaxation we applied basic molecular mechanics calculations (MM+ force field of the Hyperchem 7.5 molecular modeling package) to optimize the geometry of Co-TPP moieties.

Acknowledgements

Work supported by Canada Foundation for Innovation, British Columbia Knowledge and Development Fund, the Canadian National Science and Engineering Research Council (NSERC), and the ESF-EUROCORES-SONS Project "FunSMARTs". W.A., A.W.-B., and S.L. acknowledge scholarships from Swiss National Science Foundation, Deutscher Akademischer Austauschdienst, and NSERC, respectively. We appreciate stimulating discussions with G. A. Sawatzky, A. P. Seitsonen, W. A. Hofer, L. A. Zotti, software support from R. Fasel, O. Gröning, and M. Ruben, G. Zoppellaro for providing an initial batch of Co-TPP.

Keywords: electronic structure · NEXAFS spectroscopy · porphyrins · scanning probe microscopy · single-molecule studies

[1] R. H. Holm, P. Kennepohl, E. I. Solomon, *Chem. Rev.* **1996**, *96*, 2239–2314.
[2] J. T. Groves, *Proc. Natl. Acad. Sci.* **2003**, *100*, 3569–3574.
[3] W.-D. Woggon, *Acc. Chem. Res.* **2005**, *38*, 127–136.
[4] J. A. Shelnutt, X.-Z. Song, J. G. Ma, S.-L. Jia, W. Jentzen, C. J. Medforth, *Chem. Soc. Rev.* **1998**, *27*, 31–41.
[5] M. O. Senge, *Chem. Commun.* **2006**, 243–256.

[6] A. Hoshino, S. Isoda, H. Kuruta, T. Kobayashi, *J. Appl. Phys.* **1994**, *76*, 4113–4120.
[7] V. M. Hallmark, S. Chiang, K.-P. Meinhardt, K. Hafner, *Phys. Rev. Lett.* **1993**, *70*, 3740–3743.
[8] J. I. Pascual, J. Gomez-Herrero, C. Rogero, A. M. Baro, D. Sanchez-Portal, E. Artacho, P. Ordejon, J. M. Soler, *Chem. Phys. Lett.* **2000**, *321*, 78–82.
[9] J. Repp, G. Meyer, S. M. Stojkovic, A. Gourdon, C. Joachim, *Phys. Rev. Lett.* **2005**, *94*, 026803.
[10] X. H. Lu, M. Grobis, K. H. Khoo, S. G. Louie, M. F. Crommie, *Phys. Rev. Lett.* **2003**, *90*, 096802.
[11] X. H. Lu, M. Grobis, K. H. Khoo, S. G. Louie, M. F. Crommie, *Phys. Rev. B.* **2004**, *70*, 115418.
[12] R. Fasel, P. Aebi, R. G. Agostino, D. Naumovic, J. Osterwalder, A. Santaniello, L. Schlapbach, *Phys. Rev. Lett.* **1996**, *76*, 4733–4736.
[13] J. Weckesser, C. Cepek, R. Fasel, J. V. Barth, F. Baumberger, T. Greber, K. Kern, *J. Chem. Phys.* **2001**, *115*, 9001–9009.
[14] T. A. Jung, R. R. Schlittler, J. K. Gimzewski, *Nature* **1997**, *386*, 696.
[15] T. Yokoyama, S. Yokoyama, T. Kamikado, S. Mashiko, *J. Chem. Phys.* **2001**, *115*, 3814.
[16] W. Auwärter, A. Weber-Bargioni, A. Schiffrin, A. Riemann, O. Gröning, R. Fasel, J. V. Barth *J. Chem. Phys.* **2006**, *124*, 194708.
[17] W. Auwärter, A. Weber-Bargioni, S. Brink, A. Riemann, A. Schiffrin, M. Ruben, J. V. Barth, *ChemPhysChem* **2007**, *8*, 250–254.
[18] F. Moresco, G. Meyer, K. H. Rieder, H. Tang, A. Gourdon, C. Joachim, *Phys. Rev. Lett.* **2001**, *86*, 672–675.
[19] X. H. Qiu, G. V. Nazin, W. Ho, *Phys. Rev. Lett.* **2004**, *93*, 196806.
[20] J. V. Barth, G. Costantini, K. Kern, *Nature* **2005**, *437*, 671–679.
[21] D. Bonifazi, H. Spillmann, A. Kiebele, M. D. Wild, P. Seiler, F. Cheng, H.-J. Güntherodt, T. Jung, F. Diederich, *Angew. Chem.* **2004**, *116*, 4863–4867; *Angew. Chem. Int. Ed.* **2004**, *43*, 4759–4763.
[22] J. V. Barth *Annu. Rev. Phys. Chem.* **2007**, *58*, 375–407.
[23] H. Spillmann, A. Kiebele, T. A. Jung, D. Bonifazi, F. Cheng, F. Diederich, *Adv. Mater.* **2006**, *18*, 275–279.
[24] V. Iancu, A. Deshpande, S.-W. Hla, *Phys. Rev. Lett.* **2006**, *97*, 266603.
[25] L. Scudiero, D. E. Barlow, U. Mazur, K. W. Hipps, *J. Am. Chem. Soc.* **2001**, *123*, 4073–4080.
[26] K. Leung, S. B. Rempe, P. A. Schultz, E. M. Sproviero, V. S. Batista, M. E. Chandross, C. J. Medforth, *J. Am. Chem. Soc.* **2006**, *128*, 3659–3668.
[27] J. Stöhr, *NEXAFS Spectroscopy*, Springer, Heidelberg, **1991**.
[28] M. P. de Jong, R. Friedlein, S. L. Sorensen, G. Öhrwall, W. Osikowicz, C. Tengsted, S. K. M. Jönsson, M. Fahlman, W. R. Salaneck, *Phys. Rev. B.* **2005**, *72*, 035448.
[29] C. Castellarin, C. C. Cudia, P. Vilmercati, R. Larciprete, C. Cepek, G. Zampieri, L. Sangaletti, S. Pagliara, A. Verdini, A. Cossaro, L. Floreano, A. Morgante, L. Petaccia, S. Lizzit, C. Battocchio, G. Polzonetti, A. Goldoni, *Surf. Sci.* **2006**, *600*, 4013–4017.
[30] H. Uji-i, A. Miura, A. Schenning, E. W. Meijer, Z. Chen, F. Würthner, F. C. De Schryver, M. Van der Auweraer, S. De Feyter, *ChemPhysChem* **2006**, *6*, 2389–2395.
[31] K. M. Kadish, N. Guo, E. van Caemelbacke, R. Paolesse, D. Monti, P. Tagliatesta, *J. Porphyrins Phthalocyanines* **1998**, *2*, 439–450.
[32] M.-S. Liao, S. Scheiner, *J. Chem. Phys.* **2002**, *117*, 205–219.
[33] R. Hesper, L. H. Tjeng, G. A. Sawatzky, *Europhys. Lett.* **1997**, *40*, 177–182.
[34] J. B. Neaton, M. S. Hybertsen, S. G. Louie, *Phys. Rev. Lett.* **2006**, *97*, 216405.
[35] W. Auwärter, F. Klappenberger, A. Weber-Bargioni, A. Schiffrin, T. Strunskus, C. Wöll, Y. Pennec, A. Riemann, J. V. Barth, *J. Am. Chem. Soc.* **2007**, *129*, 11279–11285.
[36] L. A. Zotti, G. Teobaldi, W. A. Hofer, W. Auwärter, A. Weber-Bargioni, J. V. Barth, *Surf. Sci.* **2007**, *601*, 2409–2414.
[37] O. Gröning, R. Fasel in STM generator software, personal communication.
[38] R. Fasel, M. Parschau, K.-H. Ernst, *Nature* **2006**, *439*, 449–452.
[39] T. Lukasczyk, K. Flechtner, L. R. Merte, N. Jux, F. Maier, J. M. Gottfried, H.-P. Steinrück, *J. Phys. Chem. C* **2007**, *111*, 3090–3098.
[40] M. E. Cañas-Ventura, F. Klappenberger, S. Clair, S. Pons, H. Brune, K. Kern, T. Strunskus, C. Wöll, R. Fasel, J. V. Barth, *J. Chem. Phys.* **2006**, *125*, 184710.

Received: September 6, 2007
Published online on December 13, 2007

